1 **Single-Macromolecular Level Imaging of a Hydrogel Structure**
2

3 *Ryuji Kiyama, Takayuki Nonoyama, Tomas Sedlacik, Hiroshi Jinnai, and Jian Ping Gong*[*]
4

5 R. Kiyama, Graduate School of Life Science, Hokkaido University, Sapporo 001-0021, Japan
6

7 Prof. T. Nonoyama, Dr. T. Sedlacik, Prof. J. P. Gong, Faculty of Advanced Life Science,
8 Hokkaido University, Sapporo 001-0021, Japan
9

10 Prof. T. Nonoyama, Dr. T. Sedlacik, Prof. J. P. Gong, Global Station for Soft Matter, Global
11 Institution for Collaborative Research and Education (GI-CoRE), Hokkaido University,
12 Sapporo 001-0021, Japan
13

14 Prof. H Jinnai, Institute of Multidisciplinary Research for Advanced Materials, Tohoku
15 University, Sendai 980-8577, Japan
16

17 Prof. J. P. Gong, Institute for Chemical Reaction Design and Discovery (WPI-ICReDD),
18 Hokkaido University, Sapporo, 001-0021, Japan
19 Tel: +81-11-706-9011; E-mail: gong@sci.hokudai.ac.jp
20

23

24 Hydrogels are promising materials for several applications, including cell scaffolds and

25 artificial load-bearing substitutes (cartilages, ligaments, tendons, etc.). Direct observation of

26 the nanoscale polymer network of hydrogels is essential in understanding its properties.

27 However, imaging of individual network strands at the molecular level is not achieved yet due

28 to the lack of suitable methods. Herein, for the first time, we developed a novel mineral-

29 staining method and network fixation method for transmission electron microscopy

30 observation to visualize the hydrogel network in its unperturbed conformation with nanometer

31   resolution. Surface network observation indicates that the length of surface dangling chains,

32   which play a major role in friction and wetting, can be estimated from the gel mesh size.

33   Moreover, bulk observations reveals a hierarchical formation mechanism of gel heterogeneity.

34   These observations have the great potential to advance gel science by providing

35   comprehensive perspective that link bulk gel properties with nanoscale.

36

37   **1. Introduction**

38   Hydrogel is a water-abundant three-dimensional polymer network that is a promising

39   soft material for various applications, including bioengineering, soft robotics, and stretchable

40   electronics, owing to its high water content, low friction, permeability of small molecules and

41   ions, flexibility, and biocompatibility[1–4]. The surface and bulk properties of hydrogels

42   strongly depend on their molecular structure. However, state-of-the-art approaches to

43   characterise the hydrogel network structure, especially synthetic hydrogel, are still limited at

44   the average structure level derived from bulk measurements, such as the mesh size of a

45   network is determined from the bulk modulus or X-ray/light scattering[5–7].

46   Direct observation of individual network strands at the molecular level is yet to be

47   achieved due to insufficient suitable methods. Transmission electron microscopy (TEM) and

48   atomic force microscopy (AFM) are the most commonly used imaging techniques to directly

49   observe the nanostructures of materials. Compared to AFM, TEM is more suitable for gels as

it can eliminate the influence of the thermal motion of the network using resin substitution or water freezing at cryogenic temperatures[8,9]. However, existing TEM observation methods, such as electron staining, phase contrast, and scanning TEM[10–13], cannot produce a sufficient contrast for chemical gels consisting of thin polymer chains; therefore, a contrast enhancement method is desired. We considered the development of an improved staining method to be the most promising approach in terms of simplicity and contrast enhancement efficiency.
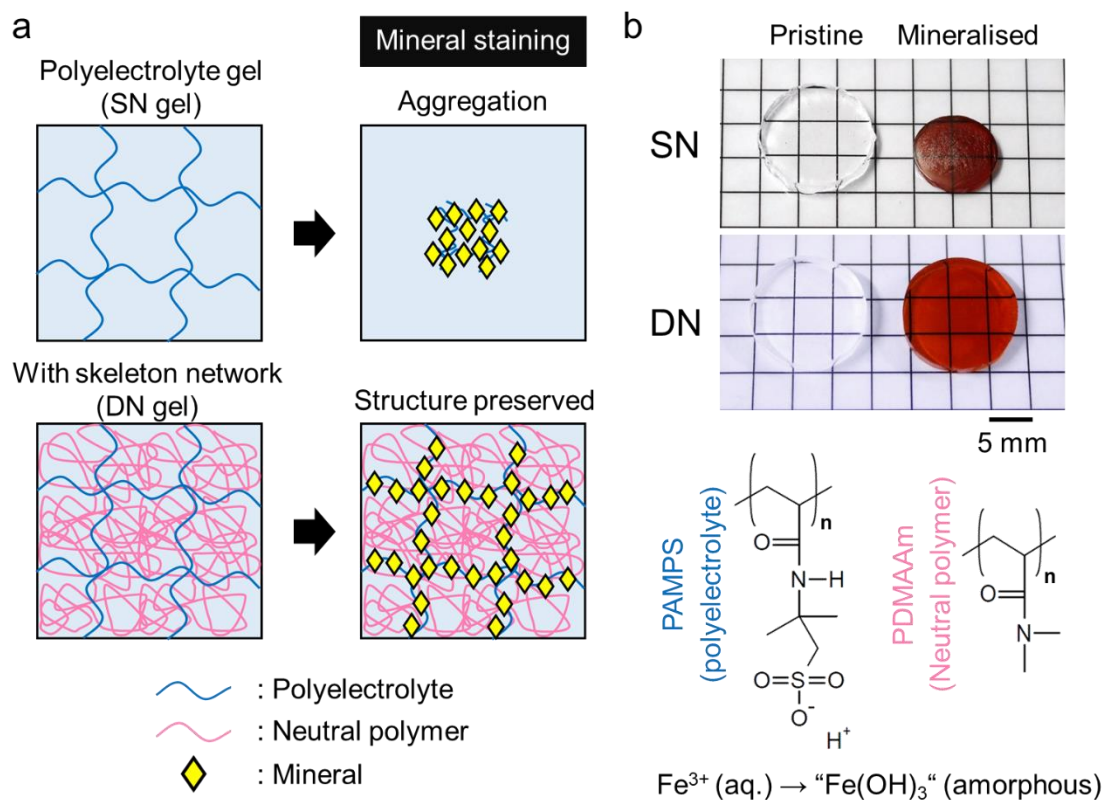
Here, we developed a novel staining method for the TEM imaging of a network structure of synthetic polyelectrolyte hydrogels in the unperturbed state with approximately 10 nm resolution. We introduced a skeleton neutral polymer network in the polyelectrolyte hydrogel to fix the conformation of the polyelectrolyte strands during specimen preparation. We adopted the mineralization of amorphous ferric oxide (AFO) nanoparticles to stain the polyelectrolyte strands in the unperturbed state. This method allowed the imaging of a network structure in a wide mesh size range (tens to hundreds of nanometers) for the first time and surface molecular structure of hydrogels. These observations provide important insights for the friction and fracture of hydrogels.

2. Results and Discussion

2.1. Mineral nanoparticle staining and double-network fixation method

3

69　　　　A conventional electron stain (Osmium (VIII) oxide) that labels one carbon–carbon

70　double bond with one heavy atom does not provide enough contrast to the sparse and

71　extremely thin network of hydrogels. Thus, we used inorganic nanoparticles as a bigger

72　marker.

73　　　　To accurately attach the nanoparticles to hydrogel network, we used the

74　heterogeneous nucleation of ferric oxide[14]. Poly(2-acrylamido-2-methyl propanesulfonic

75　acid) (PAMPS) hydrogel was adopted since sulfonic acid functional groups are expected to

76　function as nucleation points for the growth of ferric oxide particles. PAMPS gel was

77　synthesized by radical Figzation, resulting in its significant swelling in water due to its

78　polyelectrolyte nature, thereby reaching a polymer weight fraction as low as 0.3–5 wt.%. The

79　heterogeneous nucleation of amorphous ferric oxide was gently performed in the gel by iron

80　(III) hydrolysis and nano-sized AFO particles grew along the polymer network (**Figure 1a**).

81　However, this AFO deposition caused significant irreversible shrinking of the PAMPS gel due

82　to the high ionic osmotic pressure of the stain solution and intermolecular cross-linking

83　(**Figure 1b and Figure S1**). Therefore, direct AFO deposition on a single PAMPS gel

84　network can cause the collapse and aggregation of the polymer strands in the gel.

85

86

Figure 1. (**a**) Schematic illustration of the double-network method to stain a polyelectrolyte

hydrogel without causing a collapse of the polymer network strands. (**b**) Appearance of the

PAMPS-4 single network gel (SN) and double-network gel (DN) with

poly(dimethylacrylamide) (PDMAAm) before and after mineral staining (upper), and

chemical structure of PAMPS and PDMAAm, and the mineralization reaction during staining

(lower).

      To prevent network structure changes during staining, we applied the double-network

(DN) method. DN method was originally developed to toughen the brittle polyelectrolyte gels

by inducing excess amount of neutral polymer network into the polyelectrolyte gel[15–17]. In

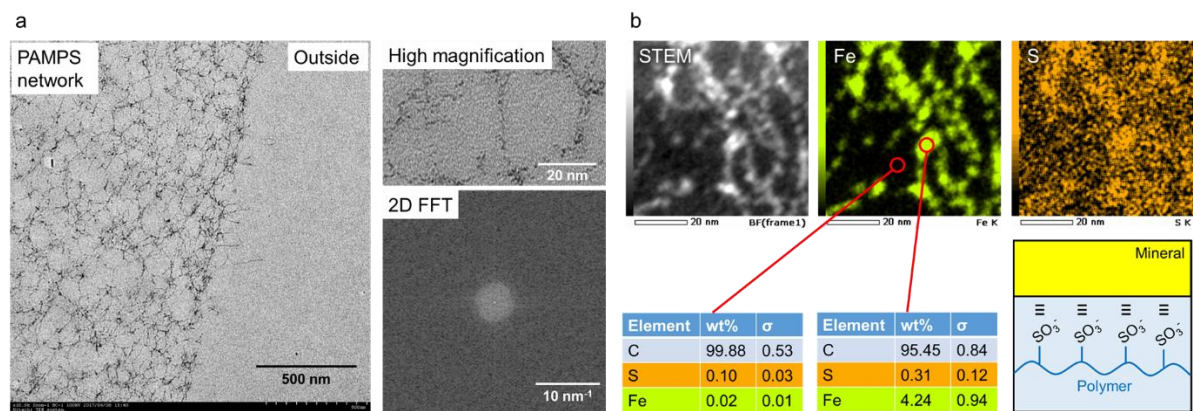this study, we applied this method to fix the target structure of the polyelectrolyte hydrogel.

97   As the skeleton neutral polymer network, poly(dimethylacrylamide) (PDMAAm), which is

98   non-reactive to the staining solution, was polymerized in excess in the PAMPS hydrogel prior

99   to AFO staining. By creating this interpenetrating DN structure with strong topological

100   entanglement, the shrinking of the PAMPS network during staining is suppressed, as

101   demonstrated by the small change in its gel size (**Figure 1a and 1b**). This is attributed to the

102   neutral PDMAAm network that generates a large osmotic pressure to maintain gel

103   swelling[18]. DN method is applicable to any polymer network. For this study, PDMAAm can

104   maintain approximately the same volume of the specimen even in the resin solution for

105   substitution. **Figure S1** shows the detailed change in thickness of the PAMPS gels in each

106   experimental step. The final thickness change is less than 10% for all PAMPS gel samples

107   prepared with different formulations, indicating that the strands of the PAMPS gel was nearly

108   unperturbed in the TEM specimen.

109

110   **2.2. Nanoscale TEM observation of the hydrogel network**

111   To confirm that AFO selectively mineralized only the PAMPS network, the PAMPS

112   micro-gels embedded in the PDMAAm gel matrix were stained[19]. **Figure S2** shows the

113   optical microscopic image of the PAMPS micro-gels, TEM images of PAMPS micro-gels in

114   the PDMAAm gel, and their corresponding schematic illustrations. The PAMPS micro-gels

115   before mineralization (not shown in the figure) are unseen by TEM, while spherical micro-

6

116   gels with several micrometer diameters are clearly identified after mineralization. This

117   confirms that AFO selectively stained the PAMPS network, but not the PDMAAm network

118   since the sulfonic group of PAMPS can catalyse the AFO deposition.

119   During staining, insufficient mineral binding to the PAMPS network results in

120   understaining. To obtain the best TEM image, we prepared a supermacroporous sponge-like

121   PAMPS/PDMAAm hydrogel comprising an interconnected porous structure with thin gel

122   walls[20], thereby supplying iron ions faster than that for bulk gel. In this sample, sufficient

123   minerals were attached to the gel mesh. The TEM micrograph shows the finest network

124   morphology of the PAMPS in this study **(Figure 2a)**. Under high magnification, it is clearly

125   observed that AFO nanoparticles with a diameter of several nanometers form network

126   structure with a mesh size of several tens of nanometers.

127

128

129   **Figure 2.** (**a**) Low and high magnification TEM images of the PAMPS gel and 2D FFT from a

130   single mineral nanoparticle. (**b**) STEM elemental mapping of the PAMPS gel. Fe and S shows

131   the iron in the ferric oxide nanoparticles and sulphur in the PAMPS gel network, respectively.

132   A supermacroporous PAMPS gel with a wall thickness of approximately 10 µm was used for

133   the observation.

134   The two-dimensional Fourier transform image of a single nanoparticle has no obvious

135   peaks (lower right in **Figure 2a**), indicating its amorphous nature. Furthermore, 3D TEM was

136   performed to obtain a 3D network structure (**Supplementary Video**)[21], clearly presenting the

137   3D connections of the network. Notably, this is the first 3D nanoscale direct observation of a

138   hydrogel network structure. To prove that only the PAMPS network was mineral stained at the

139   nanoscale, element mapping (STEM–EDS) was carried out (**Figure 2b**). The positions of

140   sulphur of PAMPS and iron of AFO overlap with each other on the nanoscale, confirming that

141   only the PAMPS network was selectively stained with ferric oxide.

142   The high magnification TEM observation of the bulk non-porous PAMPS/PDMAAm

143   gel is shown in **Figure S3**. A fine PAMPS network morphology is observed with the mesh

144   sized in tens of nanometers, which roughly agrees with the previously reported average mesh

145   size from small-angle X-ray scattering and mechanical estimation[22]. Considering the

146   polymer mesh size and thickness of the specimen slice (100 nm), the discontinuity of the

147   network can be attributed to the mesh structure that is frequently larger than thickness of the

148   specimen. The accumulative strand length in the volume of the measured view

149   ($1200 \times 1200 \times 100$ nm^3) is 9100 ± 2100 nm, which is approximately 1/10 of the contour length

150   of 1.3×10^5 nm calculated from the total amount of PAMPS in the viewing volume (**Figure**
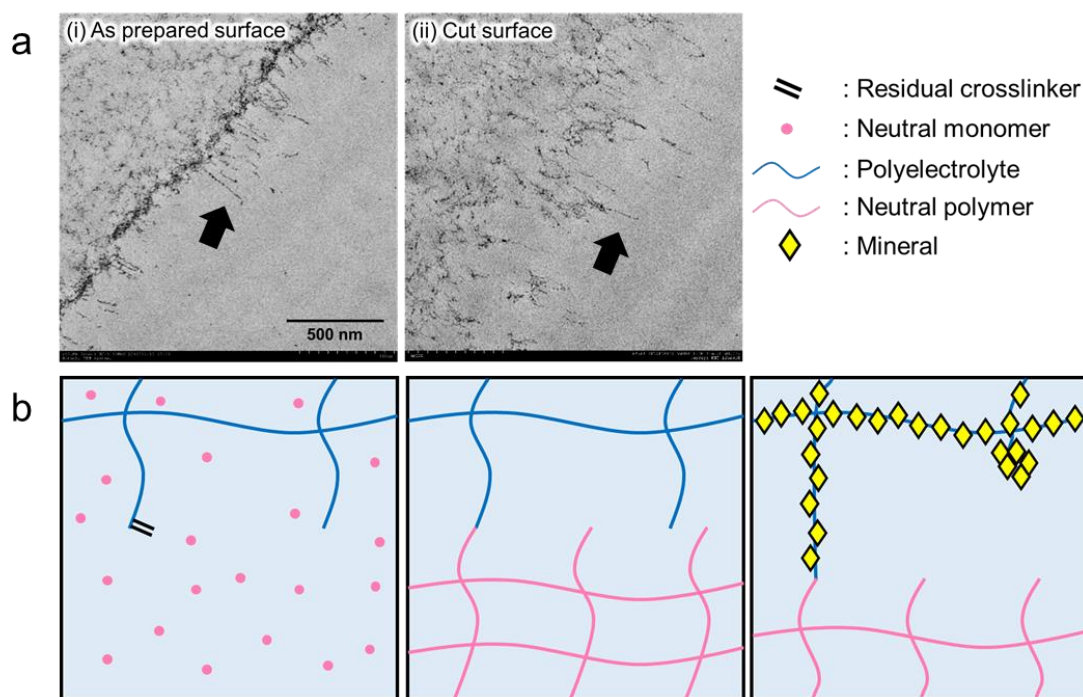
151 **S3a**). Even considering that TEM measured a 2D projected length of approximately 0.64 the

152 true length, there is still a large difference from the calculated value. These indicate that the

153 observed accumulative strand length does not represent the full contour length of the polymer

154 network and the fine structures of the polymer strands, such as blobs, were not included.

155 Moreover, the dangling chains that should be in a collapsed conformation (**Figure S3b**) are

156 also not included in the observed accumulative strand length. On the other hand, this

157 measurement provides a rough answer to the big question in the gel field, what percentage of

158 polymer chains are effective network (not dangling chains). For example, in this gel, at least

159 one-sixth or more of the polymer chains (which probably be more than one-third because the

160 real chains are loose and not fully extended) function as effective network. The TEM images

161 of the PAMPS hydrogel prepared with different crosslinker densities are shown in **Figure S4**.

162 The polymer density increases with increasing crosslinker density. In addition, the structure

163 becomes finer, while the network morphology is unclear owing to the insufficient amount of

164 mineral precursor to stain all polymer strands. These demonstrate that we achieved the direct

165 observation of an actual hydrogel polymer-network structure for the first time. This method

166 was then applied to characterise the surface and bulk structure of hydrogels.

167

168 **2.3. Surface structure of hydrogel**

169   The surface feature, such as low friction, adhesions, and permeability for small

170   molecules and ions, is an important characteristic of hydrogel materials. In nature, hyaline

171   cartilage exhibits both incredibly low friction property and semipermeability that allows

172   nutrient diffusion[23,24]. The TEM observation of the specimen prepared by our method for the

173   first time revealed the precise structure of the polymer strands at the hydrogel surface. **Figure**

174   **3A(i)** shows the outermost as-prepared surface of a PAMPS hydrogel synthesized on a flat

175   glass mold. PDMAAm was induced by second polymerization with the method described in

176   the previous section. Several hundred nanometer-sized dangling chains (indicated by the

177   black arrows) in the fully elongated state from the bulk region are observed. These surface

178   dangling chains do not collapse as they are covalently connected to the PDMAAm network

179   and are stretched by its swelling (**Figure 3a(i)**). As illustrated in **Figure 3b**, the PAMPS

180   network usually has a few unreacted vinyl groups after PAMPS polymerization[25]. During the

181   polymerization of the second skeleton network, some dangling chains with remaining vinyl

182   groups on the PAMPS gel surface are incorporated into the PDMAAm network. Therefore,

183   the surface of the formed PAMPS/PDMAAm DN hydrogel is covered by the second

184   PDMAAm network partially connected with the PAMPS dangling chains[26]. The immersion

185   of the PAMPS/PDMAAm gel in water induces the swelling of the PDMAAm network surface

186   layer and stretching of the connected PAMPS strands. In **Figure 3a(i)**, the approximate length

187   of the dangling chains (several hundred nanometers) is approximately equal as that of the

188   network mesh size in the bulk region. Therefore, these dangling strands can be assumed to be

189   strands that could not find a cross-linking partner at one end. In addition, this result indicates

190   that the length of the surface dangling chain of the chemically crosslinked gel is comparable

191   to the bulk network mesh size; thus, the length of the dangling chains of the gel surface can be

192   estimated based on the mesh size of the bulk network. It should be noted that only dangling

193   chains that are covalently connected to the second network are observed as elongated strands.

194   As most dangling chains are not covalently connected to the second network, they collapsed

195   into a globule conformation, as seen by the dark rough line on the gel surface, similar with the

196   dangling chains inside the gel (**Figure S3b**).

197

199   **Figure 3.** Surface network structure of the PAMPS-4 gel. (**a**) (i) As-prepared gel surface

200   synthesized on a flat glass mold; (ii) Surface cut with a microtome knife. The black arrows in

201   the TEM images indicate surface dangling chains. (**b**) Schematic of the surface dangling chain

202   extension by the skeleton network. The PDMAAm network in the PAMPS gel was omitted
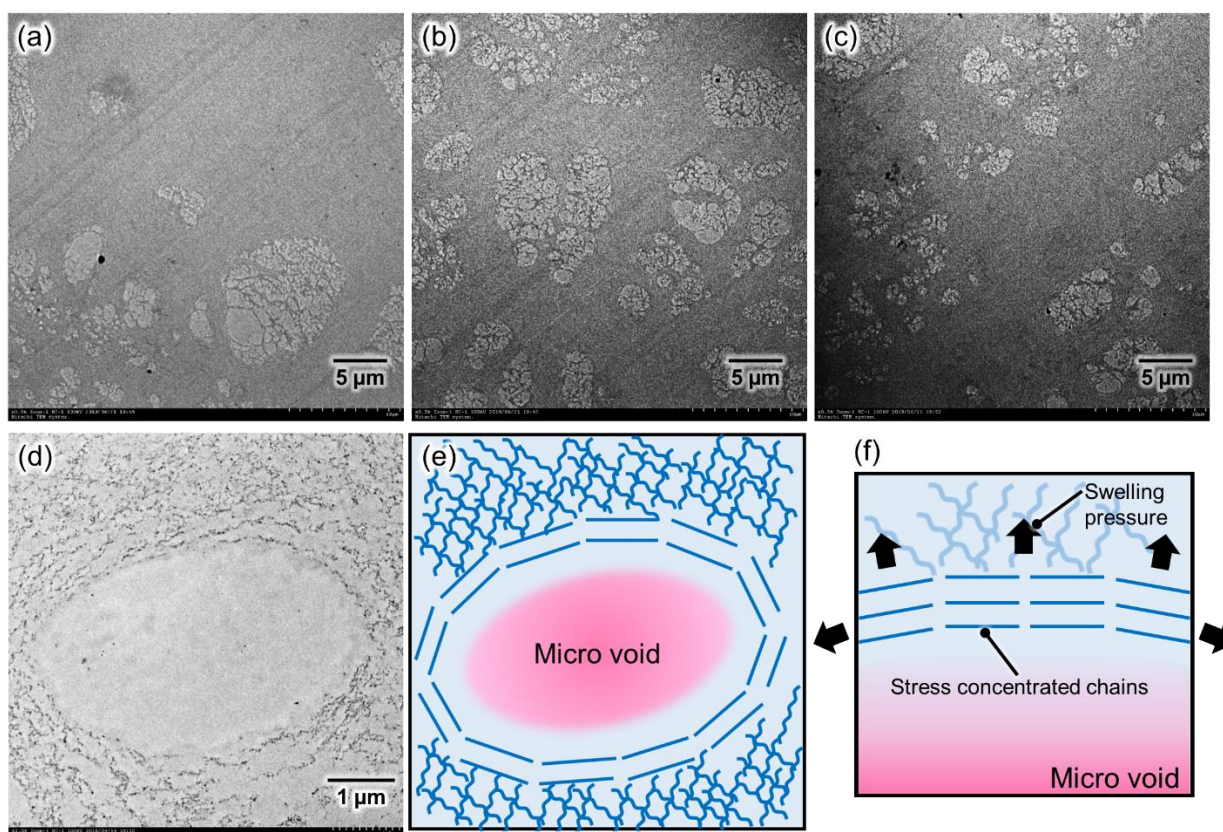
203   for schematic visibility.

204   We also observed the surface of the PAMPS gel cut using a fine microtome knife with

205   an edge thickness of 76 µm. The cut surface is significantly rougher than the as-prepared

206   surface (**Figure 3a(ii)**). In addition, it has a disordered network structure approximately 1 µm

207   deep from the outermost surface, while the mesh structure is maintained in the inner region.

208   The length of the created dangling chains at the surface is nearly equal to the bulk mesh size

209   since these dangling chains are originated from the mesh. Considering that cutting creates two

210   fracture surfaces, the damage zone has a total depth of approximately 2 µm, suggesting that

211   brittle hydrogel is fractured near the surface, despite the cutting edge thickness of 76 µm. This

212   observation can be used to estimate the relation between the microscale damage zone and

213   macroscopic fracture.

214

215   **2.4. Heterogeneity of the hydrogel**

216   The characterisation of the defects or heterogeneity is vital in understanding the

217   fracture of the material as it is governed by local structure, not by the average structure[27,28].

218   Particularly, fracture is always originated in the largest defect in a material. Here, we applied

219   the developed method to directly observe the defects in hydrogels.

220   **Figure 4** shows the TEM images of a bulk PAMPS hydrogel and its schematic

221   illustrations. The PAMPS hydrogel contains several local voids that are approximately 10 µm

222   (**Figure 4a–c**). These voids do not have a PAMPS network. The origin of defects is the

223   nonhomogeneous formation of the micro-gels[29,30]. In the initial stage of hydrogel

224   polymerization from the monomer and crosslinker, several micro-gels are instantaneously

225   formed with non-uniform spacing. When these microgels grow and coalesce together to form

226   the bulk gel, a void structure is formed where there are no micro-gels. These micro-scale

227   defects are not observed in small particle gels with a diameter of several micrometers (**Figure**

228   **S2**). Hence, a small gel is relatively homogeneous and free of large defects, while defect

229   formation is inevitable for a bulk gel, thereby affecting its mechanical properties. This

230   observation allows a simultaneous observation of the hydrogel structure at multiple scales.

231   **Figure 4d-f** shows a high magnification image of a void and its schematic illustrations.

232   Polymer strands around the void are oriented along the defect circumference, indicating that

233   these strands are highly elongated than those farther from the voids. This result denotes that

234   microscale heterogeneity, such as voids, induces nanoscale heterogeneity.

Figure 4. Micro-scale network defects in the bulk PAMPS-4 gel. (a)–(c) Low magnification

TEM images at different locations. The white areas are microvoids without a PAMPS

network. (d)–(f) High magnification TEM image around a microvoid and its schematic

illustration.

3. Conclusion

We demonstrated the combination of a novel staining method with DN technique to

directly observe a hydrogel network at the nanoscale level. The molecular structure of

polymer hydrogel in bulk and on the surface was unveiled for the first time in real space. We

clarified the presence of dangling chains on the surface of the as-prepared gels with a length

14

246   on the same scale as the mesh size. These results are important in understanding the surface

247   properties of hydrogels, including surface wetting–dewetting, sliding friction, adhesion, and

248   bonding. Furthermore, numerous micro-scale defects noted in these gels can induce stress

249   concentration of the nanoscale polymer strands. These results are essential in understanding

250   the origin of the brittleness of hydrogels. This method has the potential to be widely used not

251   only for hydrogels but also for single macromolecular level imaging of polymer materials.

252

253   **4. Experimental Methods**

254   *Materials:* The 2-acrylamido-2-methyl propanesulfonic acid (AMPS) monomer was

255   provided by Toagosei Co. Ltd, Japan. The dimethylacrylamide (DMAAm) monomer, *N, N'-*

256   methylenebisacrylamide (MBAA) crosslinker, and 2-oxoglutaric acid (α-keto) initiator, iron

257   (III) chloride hexahydrate, and iron (II) chloride tetrahydrate were purchased from Wako Pure

258   Chemical Ind., Ltd., Japan. Osmium tetroxide (OsO_4) was acquired from TAAB Laboratories

259   Equipment Ltd., England. DMAAm monomer was purified by reduced pressure distillation

260   before usage. The other chemicals were used as received. The precursor solution for the

261   PAMPS gel comprised 1 M AMPS as the monomer, 1–8 mol% MBAA as the crosslinker, and

262   0.1 mol% α-keto as the initiator. Meanwhile, the formulation of the precursor solution for the

263   PDMAAm network was 2 M DMAAm monomer, 0.1 mol% MBAA, and 0.1 mol% α-keto.

264   Each mol% is relative to the corresponding monomer.

265   *Gel synthesis:* The plate-shaped PAMPS network was synthesized from the precursor

266   solution in a mold, which was made of a 2 mm thick silicone spacer sandwiched between two

267   glass plates, by UV polymerization for 8 h in a chamber filled with inert Ar gas. Then, the

268   PAMPS gel was removed from the mold and soaked in a PDMAAm network precursor solution

269   for 1 day until reaching equilibrium. The PAMPS gel containing the PDMAAm network

270   precursor solution was sandwiched between two glass plates and irradiated with UV for its 2nd

271   polymerization for 6 h in Ar atmosphere[15]. The obtained samples were immersed in distilled

272   water for one week to completely remove residual chemicals. All glass plates used in the molds

273   were heated in a 500 °C oven for 1 h to remove any residual organics before use. The samples

274   were coded according to the PAMPS network crosslinker ratio C_{MBAA} (mol%), as PAMPS-

275   C_{MBAA}. The thickness of these swelled PAMPS gel samples were 8.99, 5.37, and 3.36 mm for

276   PAMPS-1, PAMPS-3, and PAMPS-8, respectively. PAMPS-4 micro-gels and

277   supermacroporous PAMPS-0.5 gel were prepared by suspension polymerization and

278   cryogelation using the protocols reported.[19,20] The mesh size of the supermacroporous

279   PAMPS-0.5 gel is less than that of conventional bulk PAMPS gel since the concentration of the

280   precursor solution increases with freezing in the cryogelation. The PDMAAm network in these

281   gels was introduced using the protocol described above.

282   *Compression test:* The compressive mechanical properties of the PAMPS gel were

283   examined using a mechanical tester (Tensilon RTC-1310A, Orientic Co., Japan). The samples

284   were cut into discs with 15 mm diameter using a cutting machine. The test was performed at a

285   strain rate of $1/600$ s^{-1}. Each test was performed on five samples.

286   *Mineral staining and transmission electron microscopy (TEM) observation:* For mineral

287   staining, the hydrogels were immersed in a staining solution of 2.5 M $FeCl_3$ and 1.5 M $FeCl_2$

288   mixture for 1 day at 25 °C. Subsequently, the gels were immersed in pure water to increase pH

289   and amorphous ferric oxide nanoparticles were mineralised on the PAMPS network. TEM

290   observations (H-7650, Hitachi, Japan) were performed to observe the polymer network

291   morphology of the stained hydrogels. The specimens for TEM observations were prepared by

292   freezing the hydrogels in liquid nitrogen and the water of the hydrogels was substituted with

293   ethanol and then acrylic resin (London Resin white, medium) in the chamber of an automatic

294   freeze substitution system (EM AFS2, Leica Microsystems, Germany). The gel thickness in

295   these processes is shown in **Figure** S**1**. For all PAMPS gels with different formulations, the

296   final thickness changes of the resin-cured specimen are within 10% relative to that of the

297   PAMPS gels in water. Then, 100 nm thick resin-cured specimens were cut using an ultra-

298   microtome knife (EM UC7i, Leica Microsystems, Germany) and then placed on a carbon-

299   supported copper mesh grid. The electron gun has an acceleration voltage of 100 kV.

300   Subsequently, 3D TEM and energy dispersive X-ray spectrometry were performed using a TEM

301   tomographic system (JEM-1400 and EM-05500TGP, JEOL, Japan) and scanning electron

302   microscope (JEM-F200, JEOL, Japan). The acceleration voltage of the electron guns was 120

303   and 200 kV, respectively. ImageJ software[31] was used to calculate the total chain length in the

304   TEM image of PAMPS-1.5 (**Figure S3**). The original TEM images were skeletonised and the

305   total pixels were measured in the image of five samples. This total chain length is considered

306   as the apparent length in 2D. When a three-dimensional straight line is projected in 2D, the 2D

307   apparent length can be written by the original length multiplied by $\cos\theta$, where θ is the angle of

308   the line with respect to the projection plane. The average value of $\cos\theta$ in the range of $0°$ to

309   $180°$ is $2/\pi$, which is approximately 0.64.

310   *Data analysis:* The theoretical network strand contour length was calculated from the

311   PAMPS concentration in the specimen after resin exchange. The gel composition was PAMPS-

312   1.5. The PAMPS monomer unit charged concentration at synthesis was 1 M. After equilibrium

313   swelling, staining, and resin exchange, the PAMPS-1.5 hydrogel has a volume swelling ratio of

314   166 relative to its as-prepared state. Thus, the TEM sample has a PAMPS monomer unit

315   concentration of 1/166 M. By considering the Avogadro constant of 6.02×10^{23} (mol^{-1}):

316   $$\text{Number of monomers per volume} = \frac{1}{166}\left(\frac{\text{mol}}{\text{L}}\right) \times 6.02 \times 10^{23}\ (mol^{-1})$$

317   $$= 3.6 \times 10^{24}\ (\text{monomer}/m^3).$$

318   In this experiment, the view field has a volume of $1200\times1200\times100$ nm^3 = 1.44×10^{-19} m^3. Thus,

319   $$\text{Monomer in the view field} = 3.6 \times 10^{24}\left(\frac{\text{monomer}}{m^3}\right) \times 1.44 \times 10^{-19}\ (m^3)$$

320 $= 518400 \; (monomer)$.

321   One monomer unit has a contour length of approximately 0.25 nm. Thus, the

322 theoretical network strand contour length in the fully stretched state, excluding the blob and

323 dangling chains, is:

324   Total polymer length in the view field = 518400 (monomer) × 0.25 (nm/monomer) =

325   1.3×10^5 (nm).

326

Supporting Information

328 Supporting Information is available from the Wiley Online Library or from the author.

329

341   Takeshi Higuchi (Tohoku University), Haruka Ai, and Yoshitaka Aoyama (JEOL, Japan) for

342   their kind help with the STEM measurements.

343

344   **References**

345   [1]   A. S. Hoffman, *Adv. Drug Deliv. Rev.* **2012**, *64*, 18.

346   [2]   O. Erol, A. Pantula, W. Liu, D. H. Gracias, *Adv. Mater. Technol.* **2019**, *4*, 1.

347   [3]   R. A. Green, S. Baek, L. A. Poole-Warren, P. J. Martens, *Sci. Technol. Adv. Mater.*

348   **2010**, *11*, DOI 10.1088/1468-6996/11/1/014107.

349   [4]   T. Sekitani, T. Yokota, K. Kuribara, M. Kaltenbrunner, T. Fukushima, Y. Inoue, M.

350   Sekino, T. Isoyama, Y. Abe, H. Onodera, T. Someya, *Nat. Commun.* **2016**, *7*, DOI

351   10.1038/ncomms11425.

352   [5]   M. Rubinstein, R. H. Colby, *Polymer Physics*, Oxford Univ. Press, Oxford, **2003**.

353   [6]   M. Shibayama, *Macromol. Chem. Phys.* **1998**, *199*, 1.

354   [7]   H. Furukawa, K. Horie, *Phys. Rev. E* **2003**, *68*, 1.

355   [8]   G. R. Newman, B. Jasani, E. D. Williams, *Histochem. J.* **1983**, *15*, 543.

356   [9]   N. A. Ranson, P. G. Stockley, *Emerg. Top. Phys. Virol.* **2010**, 1.

357   [10]   R. Vitali, E. Montani, *Polymer (Guildf).* **1980**, *21*, 1220.

358   [11]   H. Jinnai, T. Higuchi, X. Zhuge, A. Kumamoto, K. J. Batenburg, Y. Ikuhara, *Acc.*

359   *Chem. Res.* **2017**, *50*, 1293.

360 [12] R. Aso, H. Kurata, T. Namikoshi, T. Hashimoto, S. W. Kuo, F. C. Chang, H.

361 Hasegawa, M. Tsujimoto, M. Takano, S. Isoda, *Macromolecules* **2013**, *46*, 8589.

362 [13] M. Tosaka, R. Danev, K. Nagayama, *Macromolecules* **2005**, *38*, 7884.

363 [14] C. M. Flynn, *Chem. Rev.* **1984**, *84*, 31.

364 [15] J. Gong, Y. Katsuyama, T. Kurokawa, Y. Osada, *Adv. Mater.* **2003**, *15*, 1155.

365 [16] K. Yasuda, N. Kitamura, J. P. Gong, K. Arakaki, H. J. Kwon, S. Onodera, Y. M. Chen,

366 T. Kurokawa, F. Kanaya, Y. Ohmiya, Y. Osada, *Macromol. Biosci.* **2009**, *9*, 307.

367 [17] J. P. Gong, *Soft Matter* **2010**, *6*, 2583.

368 [18] T. Nakajima, T. Nakajima, T. Nakajima, T. Chida, K. Mito, T. Kurokawa, T.

369 Kurokawa, J. P. Gong, J. P. Gong, J. P. Gong, *Soft Matter* **2020**, *16*, 5487.

370 [19] J. Hu, K. Hiwatashi, T. Kurokawa, S. M. Liang, Z. L. Wu, J. P. Gong, *Macromolecules*

371 **2011**, *44*, 7775.

372 [20] T. Sedlačík, H. Guo, T. Nonoyama, T. Nakajima, T. Kurokawa, J. P. Gong, *Chem.*

373 *Mater.* **2020**, *32*, 8576.

374 [21] H. Jinnai, R. J. Spontak, T. Nishi, *Macromolecules* **2010**, *43*, 1675.

375 [22] K. Fukao, T. Nakajima, T. Nonoyama, T. Kurokawa, T. Kawai, J. P. Gong,

376 *Macromolecules* **2020**, *53*, 1154.

377 [23] J. Katta, Z. Jin, E. Ingham, J. Fisher, *Med. Eng. Phys.* **2008**, *30*, 1349.

378 [24] A. Jackson, W. Gu, *Curr. Rheumatol. Rev.* **2009**, *5*, 40.

379   [25]   T. Nakajima, H. Furukawa, Y. Tanaka, T. Kurokawa, Y. Osada, J. P. Gong,

380   *Macromolecules* **2009**, *42*, 2184.

381   [26]   M. Frauenlob, D. R. King, H. Guo, S. Ishihara, M. Tsuda, T. Kurokawa, H. Haga, S.

382   Tanaka, J. P. Gong, *Macromolecules* **2019**, *52*, 6704.

383   [27]   A. A. Griffith, *Masinovedenie* **1995**, *C*, 163.

384   [28]   M. Marder, J. Fineberg, *Phys. Today* **1996**, *49*, 24.

385   [29]   S. Seiffert, *Polym. Chem.* **2017**, *8*, 4472.

386   [30]   N. Ide, T. Fukuda, *Macromolecules* **1999**, *32*, 95.

387   [31]   C. A. Schneider, W. S. Rasband, K. W. Eliceiri, *Nat. Methods* **2012**, *9*, 671.
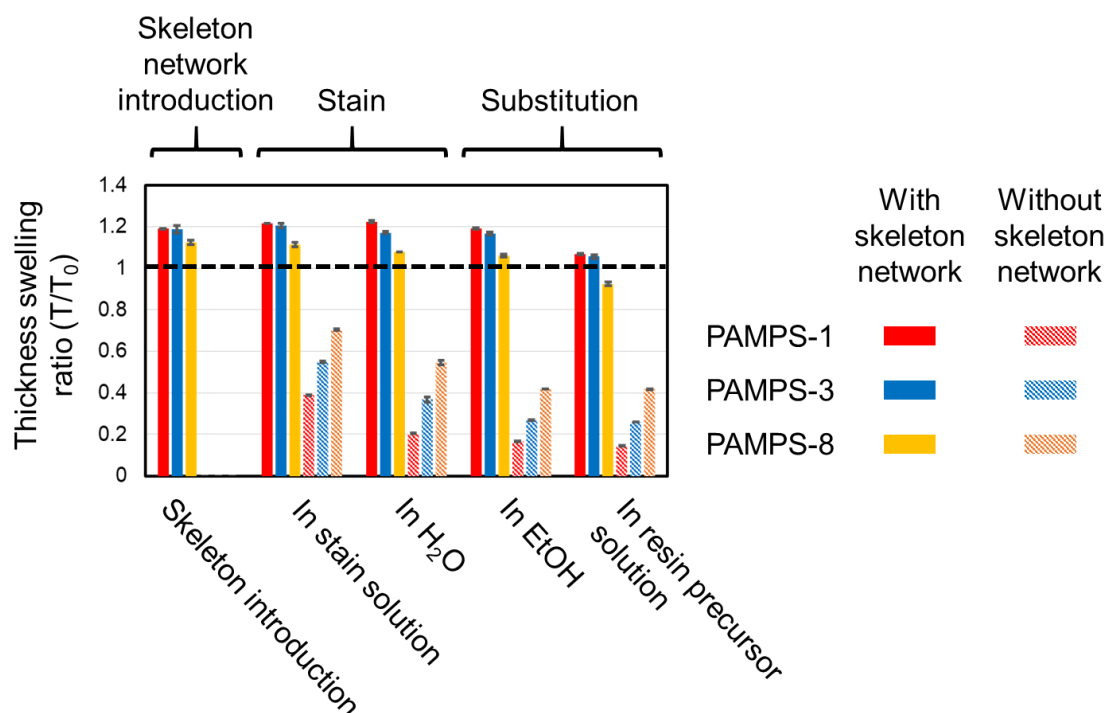
388

389

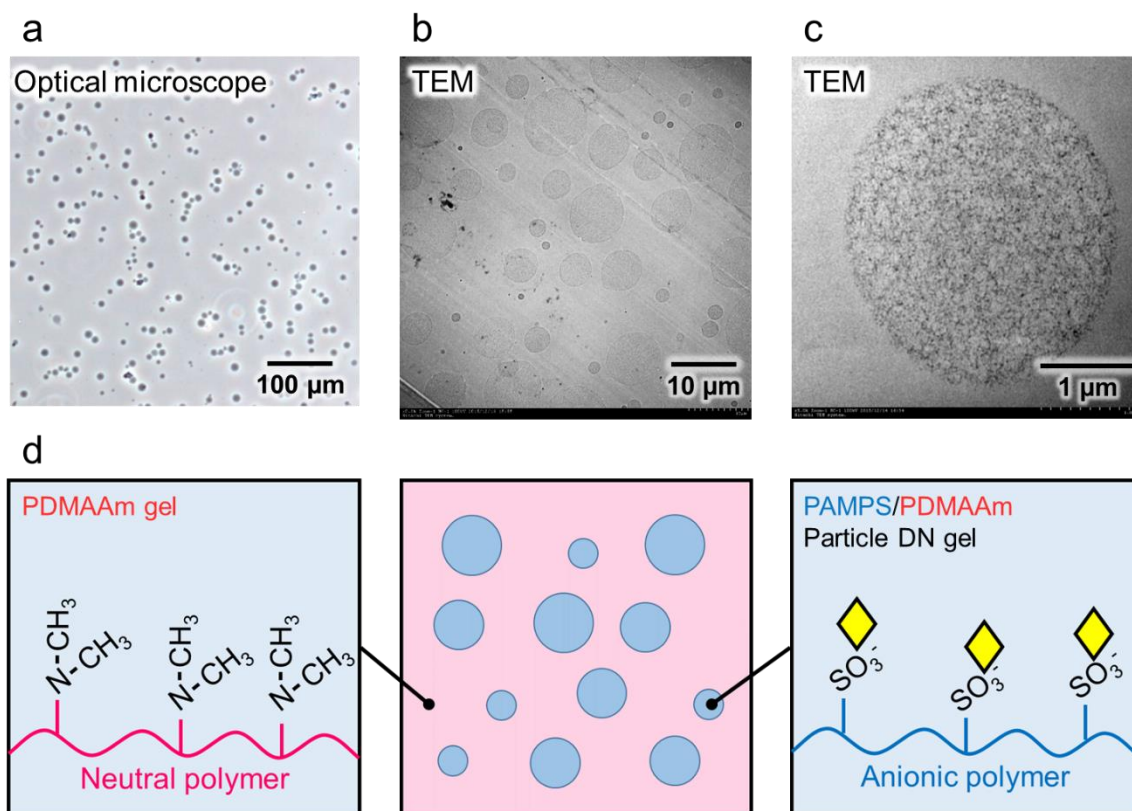390

391

392

393

394

395

396

397

Supporting Information

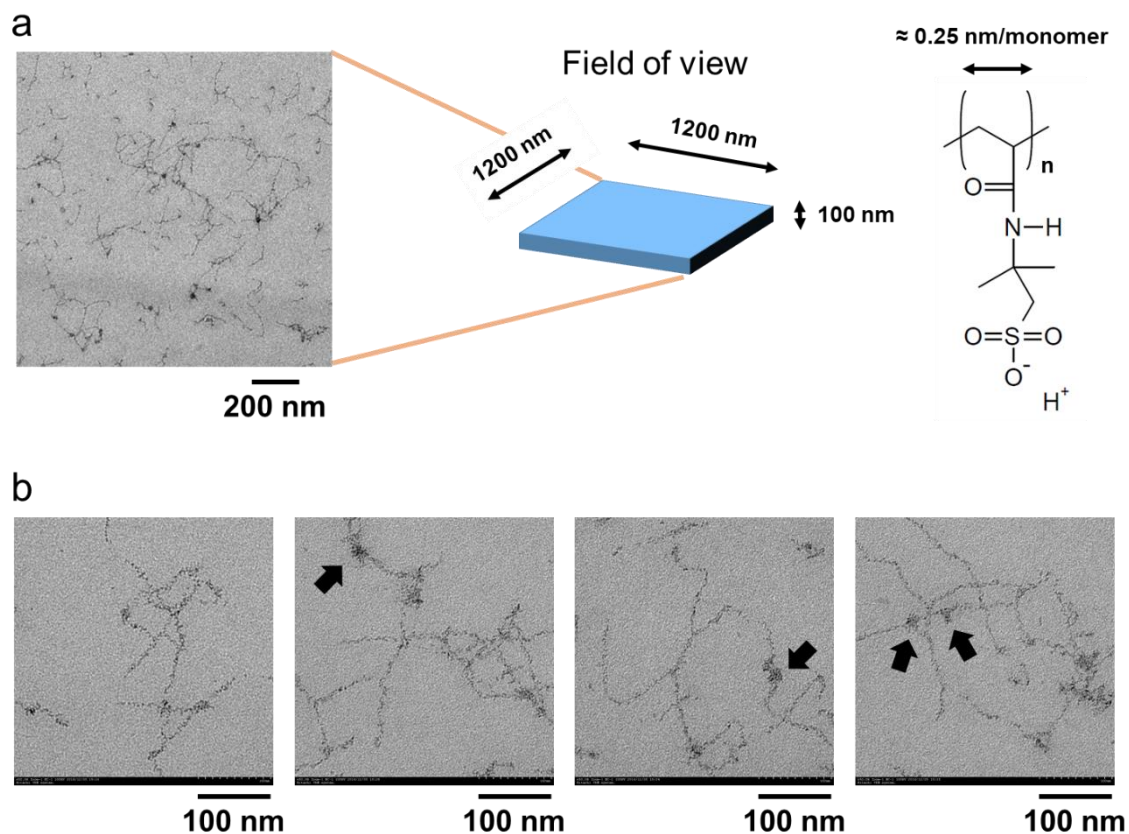**Single-Macromolecular Level Imaging of a Hydrogel Structure**

Ryuji Kiyama, Takayuki Nonoyama, Tomas Sedlacik, Hiroshi Jinnai, and Jian Ping Gong[*]

Figure S1. Thickness swelling ratio of the PAMPS gels with different crosslinker density during staining and substitution. T_0 is the thickness of the SN gels swelled in water. The black dashed line in the graph indicates the constant size ($T/T_0 = 1$). By introducing the PDMAAm skeleton, the gel swells slightly ($T/T_0 = 1.1$-1.2). The samples without a skeleton network significantly shrink ($T/T_0 = 0.1$-0.4). With the skeleton network, the change in the final size of the resin-cured specimen is within 10% ($T/T_0 = 0.9$-1.1). The error bars indicate the standard deviation for five samples.
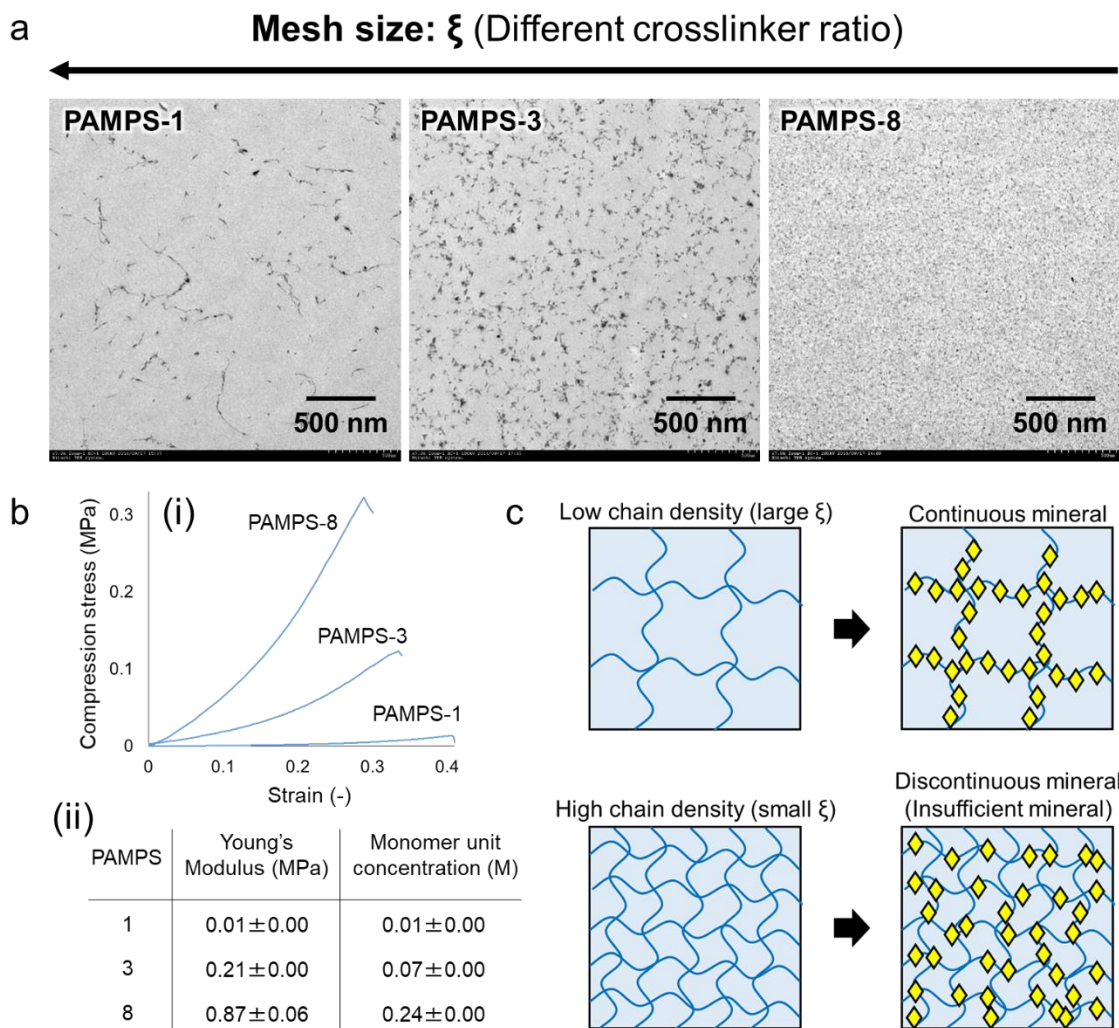
Figure S2. TEM image of the particle PAMPS-4 micro-gels in the bulk PDMAAm gel. (**a**) Optical microscopy image of the pristine PAMPS micro-gel particles. (**b**) Low magnification (×300) TEM image. (**c**) High magnification (×5000) TEM image. (**d**) Schematic illustration of (**b**).

a

Field of view

≈ 0.25 nm/monomer

1200 nm

1200 nm

100 nm

200 nm

b

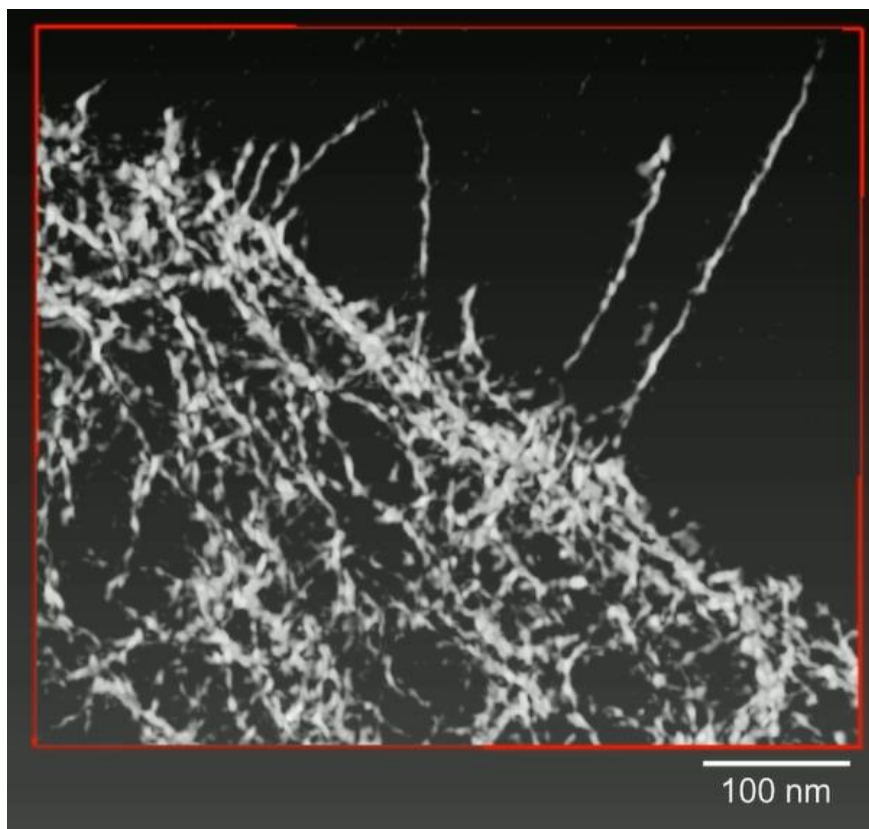100 nm   100 nm   100 nm   100 nm

429

Figure S3. (**a**) Calculation process of the polymer length in the field of view for the PAMPS-1.5 gel. The volume swelling ratio at the measured state was 166 times that of the as-prepared state for this sample. (**b**) High magnification TEM images of the PAMPS network at different locations. The mesh structures sized in tens of nanometres were clearly observed. The black arrows indicate the apparent aggregated dangling chains in the structure.

430

431

432

433

434

435

436

437

438

439

a **Mesh size: ξ** (Different crosslinker ratio)

PAMPS-1   PAMPS-3   PAMPS-8
500 nm   500 nm   500 nm

b (i)

PAMPS-8
PAMPS-3
PAMPS-1

Compression stress (MPa) — Strain (-)

(ii)

PAMPS	Young's Modulus (MPa)	Monomer unit concentration (M)
1	0.01±0.00	0.01±0.00
3	0.21±0.00	0.07±0.00
8	0.87±0.06	0.24±0.00

c Low chain density (large ξ) → Continuous mineral

High chain density (small ξ) → Discontinuous mineral (Insufficient mineral)

Figure S4. Effect of crosslinker ratio of the PAMPS gels. (a) TEM images. (b) (i) Stress–strain curves of the PAMPS gels in their water swollen state; (ii) Gel properties. (c) Illustrations of the network structure with low (upper) and high (lower) crosslinker density of the PAMPS gels before and after mineral staining.

450

451 **Supplementary Video** 3D TEM movie of the supermacroporous PAMPS gel.